

Simulations of superconducting quantum gates by digital flux tuner for qubits

Xiao Geng(耿霄), Kaiyong He(何楷泳), Jianshe Liu(刘建设), and Wei Chen(陈炜)

Citation: Chin. Phys. B, 2024, 33 (**7**): 070305. DOI: 10.1088/1674-1056/ad47ab
Journal homepage: http://cpb.iphy.ac.cn; http://iopscience.iop.org/cpb

What follows is a list of articles you may be interested in

Quantum circuit-based proxy blind signatures: A novel approach and experimental evaluation on the IBM quantum cloud platform

Xiaoping Lou(娄小平), Huiru Zan(咎慧茹), and Xuejiao Xu(徐雪娇)
Chin. Phys. B, 2024, 33 (**5**): 050307. DOI: 10.1088/1674-1056/ad22d5

Quantum correlations and entanglement in coupled optomechanical resonators with photon hopping via Gaussian interferometric power analysis

Y. Lahlou, B. Maroufi, and M. Daoud
Chin. Phys. B, 2024, 33 (**5**): 050303. DOI: 10.1088/1674-1056/ad2a6e

Remote entangling gate between a quantum dot spin and a transmon qubit mediated by microwave photons

Xing-Yu Zhu(朱行宇), Le-Tian Zhu(朱乐天), Tao Tu(涂涛), and Chuan-Feng Li(李传锋)
Chin. Phys. B, 2024, 33 (**2**): 020315. DOI: 10.1088/1674-1056/ad1747

Threshold-independent method for single-shot readout of spin qubits in semiconductor quantum dots

Rui-Zi Hu(胡睿梓), Sheng-Kai Zhu(祝圣凯), Xin Zhang(张鑫), Yuan Zhou(周圆), Ming Ni(倪铭), Rong-Long Ma(马荣龙), Gang Luo(罗刚), Zhen-Zhen Kong(孔真真), Gui-Lei Wang(王桂磊), Gang Cao(曹刚), Hai-Ou Li(李海欧), and Guo-Ping Guo(郭国平)
Chin. Phys. B, 2024, 33 (**1**): 010304. DOI: 10.1088/1674-1056/ace3a9

Improved quantum (*t*,*n*) threshold group signature

Yaodong Zhang(张耀东), Feng Liu(刘锋), and Haixin Zuo(左海新)
Chin. Phys. B, 2023, 32 (**9**): 090308. DOI: 10.1088/1674-1056/acac0a

---

Simulations of superconducting quantum gates by digital flux tuner for qubits

Xiao Geng(耿霄)[1,2,†], Kaiyong He(何楷泳)[1,2], Jianshe Liu(刘建设)[1,2], and Wei Chen(陈炜)[1,2,3,‡]

[1] *Laboratory of Superconducting Quantum Information Processing, School of Integrated Circuits, Tsinghua University, Beijing* 100084, *China*
[2] *Beijing Innovation Center for Future Chips, Tsinghua University, Beijing* 100084, *China*
[3] *Beijing National Research Center for Information Science and Technology, Beijing* 100084, *China*

(Received 19 December 2023; revised manuscript received 30 April 2024; accepted manuscript online 6 May 2024)

The interconnection bottleneck caused by limitations of cable number, inner space and cooling power of dilution refrigerators has been an outstanding challenge for building scalable superconducting quantum computers with the increasing number of qubits in quantum processors. To surmount such an obstacle, it is desirable to integrate qubits with quantum–classical interface (QCI) circuits based on rapid single flux quantum (RSFQ) circuits. In this work, a digital flux tuner for qubits (DFTQ) is proposed for manipulating flux of qubits as a crucial part of the interface circuit. A schematic diagram of the DFTQ is presented, consisting of a coarse tuning unit and a fine-tuning unit for providing magnetic flux with different precision to qubits. The method of using DFTQ to provide flux for gate operations is discussed from the optimization of circuit design and input signal. To verify the effectiveness of the method, simulations of a single DFTQ and quantum gates including a Z gate and an iSWAP gate with DFTQs are performed for flux-tunable transmons. The quantum process tomography corresponding to the two gates is also carried out to analyze the sources of gate error. The results of tomography show that the gate fidelities independent of the initial states of the Z gate and the iSWAP gate are 99.935% and 99.676%, respectively. With DFTQs inside, the QCI would be a powerful tool for building large-scale quantum computers.

Keywords: quantum computation, superconducting electronics, quantum control

PACS: 03.67.–a, 03.67.Lx, 85.25.Am **DOI:** 10.1088/1674-1056/ad47ab

1. Introduction

Superconducting quantum computers are one of the most promising approaches for realizing fault-tolerant quantum computing, with quantum processors based on Josephson qubits as their core devices.[1] Microwave systems for qubit control and readout[2] have been widely used in the manufacturing of quantum computers, enabling the execution of quantum algorithms for error correction,[3] quantum simulations[4] and achieving quantum supremacy.[5] With the increasing number of qubits, the interconnection bottleneck in microwave systems becomes an important problem because of the limitations of the number of I/O ports of quantum processors and cryogenic transmission lines.[6] To overcome the bottleneck, rapid single flux quantum (RSFQ) logic circuits[7] integrated with qubits for qubit control and readout are desirable.[8,9] This kind of RSFQ circuits can be called quantum–classical interface (QCI), which was proposed by McDermott *et al.*[10] The theory of RSFQ digital coherent XY control was studied[11–13] and the fidelities of single-qubit gate for transmons performed by SFQ pulses were measured to be about 95%[14] and improved to over 98.8% with multichip-module (MCM) architecture.[9] Two-qubit gates based on SFQ including cross-resonance (CR) gates and controlled-phase (CZ) gates were also studied.[15–18]

Flux-tunable transmons[19,20] are a kind of popular qubits in designing superconducting quantum processors, with external flux penetrating their SQUIDs as the degree of freedom for Z control. To realize digital Z control by SFQ pulses, the qubit energy tuner (QET) has been proposed by Ref. [21]. With SFQ pulses input to a pair of flux bias units (positive and negative), a QET can generate the current to provide external flux of flux-tunable transmons for Z control. However, the difference between the two inductors shunted respectively with the positive flux bias unit and the negative flux bias unit is hard to eliminate in fabrication and may cause accumulative errors of the external flux. Therefore, this article proposes an improved version of QETs, digital flux tuner for qubits (DFTQ). In a DFTQ, the two inductors are merged into a single one, which is in series with two overdamped Josephson junctions for receiving SFQ pulses. This improvement not only ensures the equality of the variations of the external flux in a step of increasing or decreasing, but also simplifies the circuit schematic diagram.

This article, in Section 2, analyzes the circuit schematic diagram of a DFTQ and discusses how the circuit generates the current providing external flux for SQUIDs of qubits. The system model for Z gate and iSWAP gate simulations is introduced and the unitary matrices of the gate operations by DFTQs are derived. In Section 3, the simulation method is elucidated, which is followed by the results and discussions of the simulations of a single DFTQ, a Z gate and an iSWAP gate.

[†]Corresponding author. E-mail: gengx19@mails.tsinghua.edu.cn
[‡]Corresponding author. E-mail: weichen@mail.tsinghua.edu.cn

© 2024 Chinese Physical Society and IOP Publishing Ltd

The standard quantum process tomography for the Z gate and the iSWAP gate is also performed to analyze the sources of gate error. Conclusions are given in Section 4.

2. Circuit and system model

Consisting of a Josephson junction and a shunted capacitor, a transmon is a qubit treated as an anharmonic oscillator with the capacitor charging energy $E_{\rm C}$ and Josephson energy $E_{\rm J}$, which decide the frequency of the transmon.[19] To perform an operation of Z control to the transmon means to change the phase of the qubit on Bloch sphere, which can be realized by changing its frequency. By replacing the single Josephson junction with a SQUID, the frequency of the transmon can be tuned with the external flux, $\Phi_{\rm e}$, provided by the current on a transmission line next to the SQUID, which actually changes the effective Josephson energy of the SQUID, $E'_{\rm J}(\Phi_{\rm e})$. Therefore, to make a DFTQ able to tune the frequency of the transmon, or the flux $\Phi_{\rm e}$, it should have the circuit elements for transforming the SFQ pulses to a current signal. To ensure the high speed and high precision of flux tuning, it should have at least two tuning units for coarse tuning and fine-tuning. This section elucidates the circuit schematic diagram of the DFTQ and the system model for simulations.

2.1. Circuit schematic diagram

The schematic of DFTQ is shown in Fig. 1, which has a coarse tuning unit and a fine-tuning unit. The coarse tuning unit is comprised of two overdamped Josephson junctions J_1 and J_2, both in series with the inductor L_{11}, which is coupled with another inductor L_{12}. The fine-tuning unit has the same circuit structure but a different mutual inductance M_2, smaller than M_1 in the coarse tuning unit, in order to tune the flux more precisely. The ports P5 and P6 are designed to be connected to the inductor $L_{\rm p}$, as shown in Fig. 1, thus making an inductor loop comprised of $L_{\rm p}$, L_{12} and L_{32}. The inductor $L_{\rm p}$ is coupled to the SQUID of a qubit with a mutual inductance M to provide the flux penetrating the SQUID, which is generated by the inductor loop current $i_{\rm p}(t)$.

The inductor loop current $i_{\rm p}(t)$ can be calculated with the following formula:

$$i_{\rm p}(t)=\frac{M_1L_{31}\left[\Phi_{\rm A}(t)-\Phi_{\rm B}(t)\right]+M_2L_{11}\left[\Phi_{\rm C}(t)-\Phi_{\rm D}(t)\right]}{L_{11}L_{31}L_{\Sigma}-M_2^2L_{11}-M_1^2L_{31}}, \quad (1)$$

where $\Phi_{\rm A}(t)$, $\Phi_{\rm B}(t)$, $\Phi_{\rm C}(t)$ and $\Phi_{\rm D}(t)$ are the integrals of the voltage at nodes A, B, C and D over the period from 0 to t, respectively. L_{Σ} is the sum of L_{12}, L_{32} and $L_{\rm p}$. The derivation for Eq. (1) is presented in Appendix A.

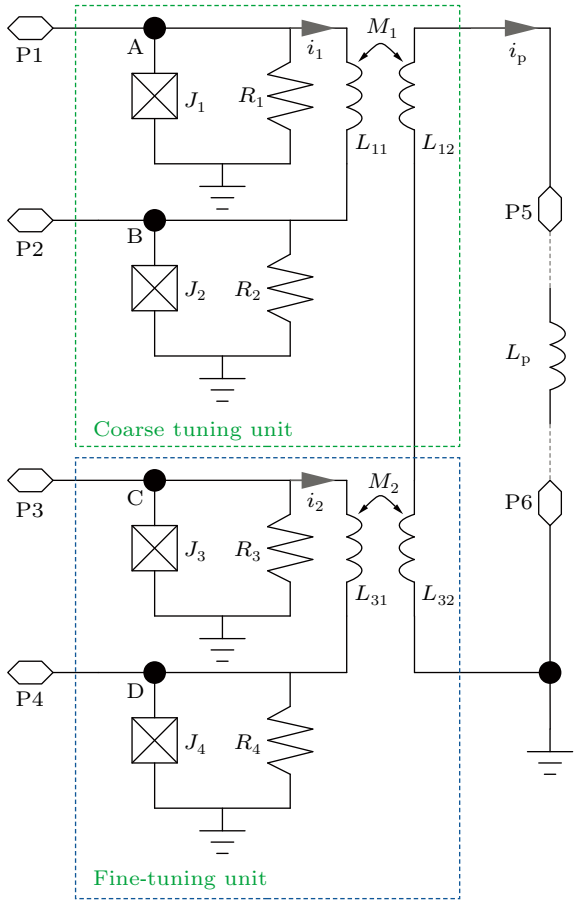


Fig. 1. The schematic of a digital flux tuner for qubits (DFTQ). P1–P4 are input ports for receiving SFQ pulses. P5 and P6 are output ports connected to the inductor $L_{\rm p}$ which provides flux for qubits.

When $\Phi_{\rm A}(t)-\Phi_{\rm B}(t)=n_{\rm c}(t)\Phi_0$ and $\Phi_{\rm C}(t)-\Phi_{\rm D}(t)=n_{\rm f}(t)\Phi_0$, that is, the number of SFQ pulses sent to P1 is $n_{\rm c}(t)$ more than that to P2 and the number of SFQ pulses sent to P3 is $n_{\rm f}(t)$ more than that to P4, there is

$$i_{\rm p}(t)=\frac{n_{\rm c}(t)M_1L_{31}\Phi_0+n_{\rm f}(t)M_2L_{11}\Phi_0}{L_{11}L_{31}L_{\Sigma}-M_2^2L_{11}-M_1^2L_{31}}. \quad (2)$$

By setting

$$\Delta i_{\rm c}=\frac{M_1L_{31}\Phi_0}{L_{11}L_{31}L_{\Sigma}-M_2^2L_{11}-M_1^2L_{31}}, \quad (3)$$

$$\Delta i_{\rm f}=\frac{M_2L_{11}\Phi_0}{L_{11}L_{31}L_{\Sigma}-M_2^2L_{11}-M_1^2L_{31}}, \quad (4)$$

the inductor loop current $i_{\rm p}(t)$ will be

$$i_{\rm p}(t)=n_{\rm c}(t)\Delta i_{\rm c}+n_{\rm f}(t)\Delta i_{\rm f}. \quad (5)$$

This means that by sending an SFQ pulse to the port P1, the current of the inductor loop $i_{\rm p}(t)$ can be increased by a specific amount $\Delta i_{\rm c}$, and then the flux provided to the qubit, $\Phi_{\rm e}$, is increased with an increment

$$\Delta\Phi_{\rm c}=M\Delta i_{\rm c}. \quad (6)$$

On the other hand, if an SFQ pulse is sent to the port P2, $i_{\rm p}(t)$ is decreased by a specific amount $\Delta i_{\rm c}$, and then $\Phi_{\rm e}$ is decreased

by $\Delta\Phi_{\rm c}$. Similar to the coarse tuning unit, the fine-tuning unit will increase (decrease) $i_{\rm p}(t)$ by a specific increment (decrement) $\Delta i_{\rm f}$ and increase (decrease) $\Phi_{\rm e}$ by

$$\Delta\Phi_{\rm f} = M\Delta i_{\rm f}, \tag{7}$$

after an SFQ pulse is sent to port P3 (P4). The flux provided to the qubit from DFTQ, $\Phi_{\rm e}$, will be

$$\Phi_{\rm e} = Mi_{\rm p}(t) = n_{\rm c}(t)\Delta\Phi_{\rm c} + n_{\rm f}(t)\Delta\Phi_{\rm f}. \tag{8}$$

Compared to a QET, the DFTQ has better repeatability of the currents providing flux or flux bias points. The current for flux tuning by a QET can be expressed by[21]

$$i_{\rm p}^{\rm QET}(t) = \frac{\Phi_0}{F}\left[n_{\rm A}(t)Y_{\rm A} - n_{\rm B}(t)Y_{\rm B} + n_{\rm C}(t)Y_{\rm C} - n_{\rm D}(t)Y_{\rm D}\right], \tag{9}$$

where $n_{\rm A}(t)$, $n_{\rm B}(t)$, $n_{\rm C}(t)$ and $n_{\rm D}(t)$ are the numbers of SFQ pulses having been sent to ports A, B, C and D of the QET at the moment t. The parameters F, $Y_{\rm A}$, $Y_{\rm B}$, $Y_{\rm C}$, $Y_{\rm D}$ are determined by circuit parameters L_i', M_i', L_{12}', L_{34}', M_{12}', M_{34}' and L_Σ' ($i = 1, 2, 3, 4$) in QET (to distinguish these circuit parameters from those of the DFTQ, they are denoted by the original symbols from Ref. [21] with additional quotation marks as superscripts):

$$\begin{aligned} F =\ & L_2'\{M_{34}'^2(L_1'L_\Sigma' - M_1'^2) + 2L_1'M_3'M_{34}'M_4' \\ & + L_3'\left[-L_4'(L_1'L_\Sigma' - M_1'^2) + L_1'M_4'^2\right] + L_1'L_4'M_3'^2\} \\ & + (-L_1'M_2'^2 - L_\Sigma'M_{12}'^2 - 2M_1'M_{12}'M_2')M_{34}'^2 \\ & - 2M_{12}'^2M_3'M_{34}'M_4' + L_3'\left[(L_1'M_2'^2 + L_\Sigma'M_{12}'^2\right. \\ & \left. + 2M_1'M_{12}'M_2')L_4' - M_{12}'^2M_4'^2\right] - L_4'M_{12}'^2M_3'^2, \end{aligned} \tag{10}$$

$$Y_{\rm A} = (L_3'L_4' - M_{34}'^2)(L_2'M_1' + M_{12}'M_2'), \tag{11}$$

$$Y_{\rm B} = (L_3'L_4' - M_{34}'^2)(L_1'M_2' + M_{12}'M_1'), \tag{12}$$

$$Y_{\rm C} = (L_1'L_2' - M_{12}'^2)(L_4'M_3' + M_{34}'M_4'), \tag{13}$$

$$Y_{\rm D} = (L_1'L_2' - M_{12}'^2)(L_3'M_4' + M_{34}'M_3'). \tag{14}$$

In the ideal situation, the current $i_{\rm p}^{\rm QET}(t)$ can get back to the reference level $i_{\rm ref} = i_{\rm p}^{\rm QET}(t_0)$, which means

$$\begin{aligned} \Delta i_{\rm p}^{\rm QET}(t,t_0) &= \frac{\Phi_0}{F}\left[\Delta n_{\rm A}Y_{\rm A} - \Delta n_{\rm B}Y_{\rm B} + \Delta n_{\rm C}Y_{\rm C} - \Delta n_{\rm D}Y_{\rm D}\right] \\ &= 0, \end{aligned} \tag{15}$$

where $\Delta i_{\rm p}^{\rm QET}(t,t_0) = i_{\rm p}^{\rm QET}(t) - i_{\rm p}^{\rm QET}(t_0)$ is the difference of the currents, and $\Delta n_{\rm A} = n_{\rm A}(t) - n_{\rm A}(t_0)$, $\Delta n_{\rm B} = n_{\rm B}(t) - n_{\rm B}(t_0)$, $\Delta n_{\rm C} = n_{\rm C}(t) - n_{\rm C}(t_0)$ and $\Delta n_{\rm D} = n_{\rm D}(t) - n_{\rm D}(t_0)$ are the differences between the cumulative numbers of SFQ pulses sent to ports A, B, C, D at the moments t and t_0, respectively. To make Eq. (15) hold, for a QET there should be

$$Y_{\rm A} = Y_{\rm B}, \tag{16}$$

$$Y_{\rm C} = Y_{\rm D}, \tag{17}$$

when it is designed and

$$\Delta n_{\rm A} = \Delta n_{\rm B}, \tag{18}$$

$$\Delta n_{\rm C} = \Delta n_{\rm D}, \tag{19}$$

when it is used. Equations (16) and (17) can be satisfied by setting $M_1' = M_2'$, $L_1' = L_2'$ and $L_3' = L_4'$. However, due to the imperfect fabrication, the inductors L_1' and L_2' (or L_3' and L_4') are difficult to be totally identical, which makes Eqs. (16) and (17) hard to be satisfied. There may be non-zero cumulative error $\Delta i_{\rm p,err} = \Delta n_{\rm A}(Y_{\rm A} - Y_{\rm B}) + \Delta n_{\rm C}(Y_{\rm C} - Y_{\rm D})$ after the operation of turning back to $i_{\rm ref}$. This problem is solved in the DFTQ where the cumulative error of current $i_{\rm p}(t)$ caused by imperfect fabrication is always 0 because Josephson junctions share the same inductor L_{11} (for coarse tuning) or L_{31} (for fine-tuning) in Fig. 1. With better repeatability of the currents providing flux or flux bias points, a DFTQ is potentially able to tune the flux of a transmon-like coupler[22] for two-qubit gate operations.

2.2. System model for simulation

To establish a concise model of Z control by DFTQs to flux-tunable transmons, the waveform of $i_{\rm p}(t)$ can be approximately described by a piecewise function $i_{\rm z}(t)$, or $i_{\rm z}(t, N_{\rm f}, N_{\rm c}, N_{\rm t})$, defined by

$$\begin{aligned} & i_{\rm z}(t, N_{\rm f}, N_{\rm c}, N_{\rm t}) \\ & = \begin{cases} i_{\rm ref} + \lceil \dfrac{t - t_{\rm s}}{\Delta t} \rceil \Delta i_{\rm f}, & t_{\rm s} \le t < t_1, \\ i_{\rm ref} + N_{\rm f}\Delta i_{\rm f} + \lceil \dfrac{t - t_1}{\Delta t} \rceil \Delta i_{\rm c}, & t_1 \le t < t_2, \\ i_{\rm ref} + N_{\rm f}\Delta i_{\rm f} + N_{\rm c}\Delta i_{\rm c}, & t_2 \le t < t_3, \\ i_{\rm ref} + N_{\rm f}\Delta i_{\rm f} + N_{\rm c}\Delta i_{\rm c} - \lceil \dfrac{t - t_3}{\Delta t} \rceil \Delta i_{\rm c}, & t_3 \le t < t_4, \\ i_{\rm ref} + N_{\rm f}\Delta i_{\rm f} - \lceil \dfrac{t - t_4}{\Delta t} \rceil, & t_4 \le t \le t_{\rm e}, \end{cases} \end{aligned} \tag{20}$$

where $t_1 = t_{\rm s} + N_{\rm f}\Delta t$, $t_2 = t_{\rm s} + (N_{\rm f} + N_{\rm c} - 1)\Delta t$, $t_3 = t_{\rm s} + (N_{\rm f} + N_{\rm c} + N_{\rm t} - 1)\Delta t$, $t_4 = t_{\rm s} + (N_{\rm f} + 2N_{\rm c} + N_{\rm t} - 2)\Delta t$, and $t_{\rm e} = t_{\rm s} + (2N_{\rm f} + 2N_{\rm c} + N_{\rm t} - 2)\Delta t$. The piecewise function $i_{\rm z}(t)$ can be called a basic waveform repeated with different parameters in an operation of Z or iSWAP. $i_{\rm z}(t)$ is changed by SFQ pulses shown in Fig. 2(a) with the total operation time $T_{\rm Z} = t_{\rm e} - t_{\rm s} = (2N_{\rm f} + 2N_{\rm c} + N_{\rm t} - 2)\Delta t$, integer times of the clock period of RSFQ circuits driving the DFTQ, Δt. The curve of $i_{\rm z}(t)$ is shown in Fig. 2(b). $i_{\rm z}(t)$ starts increasing at $t_{\rm s}$ and reaches the target value of the inductor loop current $i_{\rm target} = i_{\rm ref} + N_{\rm f}\Delta i_{\rm f} + N_{\rm c}\Delta i_{\rm c}$ with fine-tuning first and coarse tuning later. The current is maintained at $i_{\rm target}$ for a period of time $N_{\rm t}\Delta t$, which is followed by its decreasing to the reference level $i_{\rm ref}$ at $t_{\rm e}$ with coarse tuning first and fine-tuning later.

The Hamiltonian of a system composed of two flux-tunable transmons in Fig. 3(a) can be described by the following equation[19,23] with rotating wave approximation (RWA):

$$H/\hbar = \omega_{\rm q1}a_1^\dagger a_1 + \frac{\alpha_1}{2}a_1^\dagger a_1^\dagger a_1 a_1 + \omega_{\rm q2}a_2^\dagger a_2$$

$$+\frac{\alpha_2}{2}a_2^\dagger a_2^\dagger a_2 a_2 + g(a_1^\dagger a_2 + a_1 a_2^\dagger), \tag{21}$$

where $a_1^\dagger$ and a_1 are the creation and annihilation operators of qubit 1, respectively. $a_2^\dagger$ and a_2 are the creation and annihilation operators of qubit 2, respectively. ω_{q1} and ω_{q2} are respectively the bare frequencies of qubit 1 and qubit 2, which can be tuned by two DFTQs. α_1 and α_2 are their anharmonicities. g is the coupling strength dependent on qubit frequencies and the coupling capacitance C_g. Assuming that the qubit k ($k = 1, 2$) is a symmetric transmon with charging energy E_{Ck}, Josephson energy E_{Jk} and external flux Φ_{ek} provided by $i_{zk}(t)$, H can be denoted as $H(\omega_{q1}, \omega_{q2})$, or

$$H = H\left(\omega_{q1}(i_{z1}(t)), \omega_{q2}(i_{z2}(t))\right), \tag{22}$$

and the evolution operator of H from the moment t_0 to t should be

$$U(t,t_0) = \mathcal{T}\exp\left(-\frac{\mathrm{i}}{\hbar}\int_{t_0}^{t} H(\omega_{q1},\omega_{q2})\,\mathrm{d}t'\right), \tag{23}$$

where $\mathcal{T}$ is the chronological operator and

$$\omega_{qk}(i_{zk}(t)) = \frac{\left(\sqrt{8E_{Ck}\cdot 2E_{Jk}\left|\cos\left(\pi\frac{\Phi_{ek}(i_{zk}(t))}{\Phi_0}\right)\right|} - E_{Ck}\right)}{\hbar}, \tag{24}$$

$$\Phi_{ek}(i_{zk}(t)) = Mi_{zk}(t), \quad (k = 1, 2). \tag{25}$$

When the two qubits are running at the idle frequencies ω_1 and ω_2, which are far detuning, the sum of the Hamiltonians of the two qubits will be a constant:

$$H_0/\hbar = \omega_1 a_1^\dagger a_1 + \frac{\alpha_1}{2}a_1^\dagger a_1^\dagger a_1 a_1 + \omega_2 a_2^\dagger a_2 + \frac{\alpha_2}{2}a_2^\dagger a_2^\dagger a_2 a_2, \tag{26}$$

so that the unitary matrix transforming the qubits' states in stationary frame into the state in the rotating frame will be

$$U_{rf}(t,t_0) = \exp\left[\frac{\mathrm{i}}{\hbar}H_0\,(t-t_0)\right]. \tag{27}$$

Then the evolution operator of a gate in the rotating frame should be

$$\tilde{U}(t,t_0) = U_{rf}(t,t_0)U(t,t_0). \tag{28}$$

In the following analysis, when the unitary matrices of gates are derived, only the lowest two energy levels of qubits are considered, but in the simulations, the lowest three energy levels of qubits are considered and the situations of decoherence are ignored.

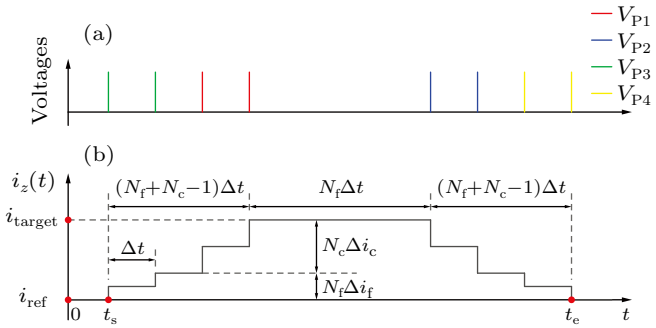
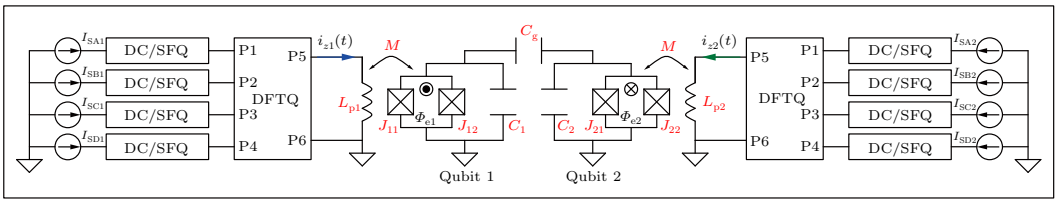


Fig. 2. Input and output signals of a DFTQ. (a) Voltages of SFQ pulses as inputs for a DFTQ. (b) The curve of $i_z(t)$ approximately describing the basic waveform of the inductor loop current $i_p(t)$. The current starts increasing at the moment t_s. With fine-tuning first and coarse tuning later, it reaches the target value $i_{target} = i_{ref} + N_f\Delta i_f + N_c\Delta i_c$ and then it is maintained for a period of time $N_t\Delta t$. Finally, by coarse tuning first and fine-tuning later, the current decreases back to reference level i_{ref} at $t_e = t_s + (2N_f + 2N_c + N_t - 2)\Delta t$. The total operation time is $T_Z = (2N_f + 2N_c + N_t - 2)\Delta t$. Here, $N_f = 2$, $N_c = 2$ and $N_t = 4$.

(a) Circuit schematic diagram for simulation of Z gates and iSWAP gates by DFTQs for two-qubit system



(b) Funtions $i_{z1}(t)$ and $i_{z2}(t)$ approximately describing the waveforms of $i_{p1}(t)$ and $i_{p2}(t)$ for iSWAP gates by DFTQs

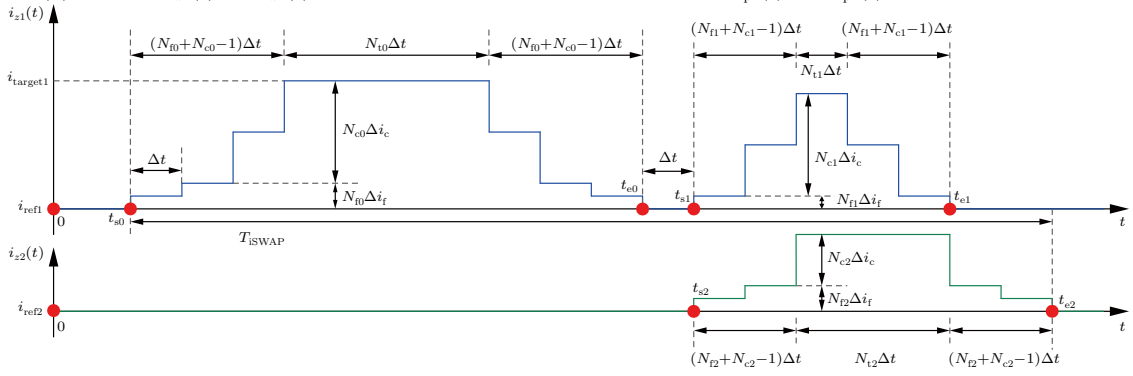


Fig. 3. Control model for simulations of Z control by DFTQs for a two-qubit system. (a) Circuit schematic diagram for simulation of Z gates and iSWAP gates by DFTQs for two-qubit system. (b) Funtions $i_{z1}(t)$ and $i_{z2}(t)$ approximately describing the waveforms of $i_{p1}(t)$ and $i_{p2}(t)$ for iSWAP gates by DFTQs. The total gate operation time is $T_{iSWAP} = \Delta t[(2N_{f0} + 2N_{c0} + N_{t0} - 2) + \max\{(2N_{f1} + 2N_{c1} + N_{t1} - 2), (2N_{f2} + 2N_{c2} + N_{t2} - 2)\} + 1]$.

2.2.1. The Z gate

We define $U_\phi(t,t_0)$ as the phase gate in the stationary frame simultaneously manipulating qubit 1 and qubit 2. When ω_{q1} and ω_{q2} are constants and far detuned, the unitary matrix of the phase gate is

$$\begin{aligned} U_\phi(t,t_0) = & |00\rangle\langle 00| + \mathrm{e}^{-\mathrm{i}\omega_{|01\rangle}(t-t_0)}|01\rangle\langle 01| \\ & + \mathrm{e}^{-\mathrm{i}\omega_{|10\rangle}(t-t_0)}|10\rangle\langle 10| \\ & + \mathrm{e}^{-\mathrm{i}\omega_{|11\rangle}(t-t_0)}|11\rangle\langle 11|, \end{aligned} \tag{29}$$

where $\omega_{|ij\rangle}$ $(i,j=1,2)$ is the difference between the frequencies of the eigen energies of the states $|ij\rangle$ and $|00\rangle$. When $\omega_{|ij\rangle}$ is changed by $i_{z1}(t)$ and $i_{z2}(t)$, it also becomes a piecewise function, which means $\omega_{|ij\rangle}$ can be obtained by calculating eigen energies corresponding to specific $i_{z1}(t)$ and $i_{z2}(t)$ and be denoted as the function of $i_{z1}(t)$ and $i_{z2}(t)$:

$$\omega_{|ij\rangle}(t) = \omega_{|ij\rangle}(i_{z1}(t), i_{z2}(t)), \tag{30}$$

and Eq. (29) should be rewritten as

$$\begin{aligned} U_\phi(t,t_0) = & |00\rangle\langle 00| + \exp\left[-\mathrm{i}\int_{t_0}^{t}\omega_{|01\rangle}(t')\mathrm{d}t'\right]|01\rangle\langle 01| \\ & + \exp\left[-\mathrm{i}\int_{t_0}^{t}\omega_{|10\rangle}(t')\mathrm{d}t'\right]|10\rangle\langle 10| \\ & + \exp\left[-\mathrm{i}\int_{t_0}^{t}\omega_{|11\rangle}(t')\mathrm{d}t'\right]|11\rangle\langle 11|. \end{aligned} \tag{31}$$

Then according to Eqs. (28) and(31), the unitary matrix of the phase gate in the rotating frame is

$$\begin{aligned} \tilde{U}_\phi(t,t_0) = & |00\rangle\langle 00| + \exp\left[\mathrm{i}\int_{t_0}^{t}(\omega_2 - \omega_{|01\rangle}(t'))\mathrm{d}t'\right]|01\rangle\langle 01| \\ & + \exp\left[\mathrm{i}\int_{t_0}^{t}(\omega_1 - \omega_{|10\rangle}(t'))\mathrm{d}t'\right]|10\rangle\langle 10| \\ & + \exp\left[\mathrm{i}\int_{t_0}^{t}(\omega_1 + \omega_2 - \omega_{|11\rangle}(t'))\mathrm{d}t'\right]|11\rangle\langle 11|. \end{aligned} \tag{32}$$

From Eq. (20), $i_{z1}(t)$ and $i_{z2}(t)$ can be obtained by substituting $\{N_{f1}, N_{c1}, N_{t1}\}$ or $\{N_{f2}, N_{c12}, N_{t2}\}$ for $\{N_f, N_c, N_t\}$ in $i_z(t, N_f, N_c, N_t)$, i.e.,

$$i_{z1}(t) = i_z(t, N_{f1}, N_{c1}, N_{t1}), \quad t_{s1} \le t \le t_{e1}, \tag{33}$$

$$i_{z2}(t) = i_z(t, N_{f2}, N_{c2}, N_{t2}), \quad t_{s2} \le t \le t_{e2}, \tag{34}$$

where the start moment $t_s = \min\{t_{s1}, t_{s2}\}$ and the end moment $t_e = \max\{t_{e1}, t_{e2}\}$. Therefore, $\tilde{U}_\phi(t_e, t_s)$ can be calculated according to Eqs. (30)–(32) and (20), and can be denoted as

$$\tilde{U}_\phi(t_e, t_s) = \tilde{U}_\phi(N_{f1}, N_{c1}, N_{t1}, N_{f2}, N_{c2}, N_{t2}). \tag{35}$$

The phase shifts of qubit 1 and qubit 2 can be respectively denoted as

$$\phi_1 = \int_{t_s}^{t_e}(\omega_1 - \omega_{|10\rangle}(t'))\,\mathrm{d}t', \tag{36}$$

$$\phi_2 = \int_{t_s}^{t_e}(\omega_2 - \omega_{|01\rangle}(t'))\,\mathrm{d}t'. \tag{37}$$

When the qubit frequencies are far detuned, there is $\omega_{|11\rangle} = \omega_{|01\rangle} + \omega_{|10\rangle}$, so that according to Eq. (31), only considering the lowest two energy levels of each qubit, there is

$$\tilde{U}_\phi(t_e, t_s) = \begin{bmatrix} 1 & 0 & 0 & 0 \\ 0 & \mathrm{e}^{\mathrm{i}\phi_2} & 0 & 0 \\ 0 & 0 & \mathrm{e}^{\mathrm{i}\phi_1} & 0 \\ 0 & 0 & 0 & \mathrm{e}^{\mathrm{i}(\phi_1+\phi_2)} \end{bmatrix}. \tag{38}$$

A Z gate for qubit k or two simultaneous Z gates for both qubits can be realized by using $\tilde{U}_\phi$. If the phase shift is $\phi_k = \pi + 2n\pi$ $(n \in \mathbb{Z},\ k = 1,2)$ for qubit k with proper parameters $N_{f1}, N_{c1}, N_{t1}, N_{f2}, N_{c2}$ and N_{t2}, then $\tilde{U}_\phi$ will be an operator of the Z gate to qubit k. The unitary matrix of ideal Z gate for only manipulating qubit 1 is

$$\tilde{U}_{\mathrm{ideal},Z1} = \begin{bmatrix} 1 & 0 & 0 & 0 \\ 0 & 1 & 0 & 0 \\ 0 & 0 & -1 & 0 \\ 0 & 0 & 0 & -1 \end{bmatrix}, \tag{39}$$

and the unitary matrix of ideal Z gate for only manipulating qubit 2 is

$$\tilde{U}_{\mathrm{ideal},Z2} = \begin{bmatrix} 1 & 0 & 0 & 0 \\ 0 & -1 & 0 & 0 \\ 0 & 0 & 1 & 0 \\ 0 & 0 & 0 & -1 \end{bmatrix}. \tag{40}$$

2.2.2. The iSWAP gate

To realize an iSWAP gate, the bare frequencies of two qubits, ω_{q1} and ω_{q2}, should be tuned at the same value. Assuming that the idle frequency ω_1 is bigger than ω_2, to decrease ω_{q1} and make $\omega_{q1} = \omega_{q2} = \omega_2$, the DFTQ for qubit 1 should provide a proper flux Φ_{e1} for qubit 1 by increasing $i_{p1}(t)$ to i_{target1}. After that $i_{p1}(t)$ should maintain at i_{target1} for a period of time to swap the states of the two qubits. Then $i_{p1}(t)$ should return back to the original value i_{ref1} to stop the swapping. Because of the phase shift of qubits and incomplete state swapping, the unitary matrix of the operations above is

$$\tilde{U}_{\mathrm{swap}} = \begin{bmatrix} 1 & 0 & 0 & 0 \\ 0 & u_{22} & u_{23} & 0 \\ 0 & u_{32} & u_{33} & 0 \\ 0 & 0 & 0 & u_{44} \end{bmatrix}, \tag{41}$$

which is realized by setting $i_{z1}(t)$ and $i_{z2}(t)$ with Eq. (20) according to Fig. 3(b):

$$i_{z1}(t) = i_z(t, N_{f0}, N_{c0}, N_{t0}), \quad t_{s0} \le t \le t_{e0}, \tag{42}$$

$$i_{z2}(t) = i_z(t, 0, 0, 0), \quad t_{s0} \le t \le t_{e0}. \tag{43}$$

The $\tilde{U}_{\mathrm{swap}}$ can be calculated according to Eqs. (20)–(28), and can be denoted as

$$\tilde{U}_{\mathrm{swap}} = \tilde{U}_{\mathrm{swap}}(N_{f0}, N_{c0}, N_{t0}). \tag{44}$$

At the end of the iSWAP gate, a specific phase shift operation $\tilde{U}_{\phi}(N_{\rm f1},N_{\rm c1},N_{\rm t1},N_{\rm f2},N_{\rm c2},N_{\rm t2})$ should be performed to make both phases of qubits equal $-\pi/2$, so that

$$\begin{aligned}&\tilde{U}_{\rm DFTQ,iSWAP}\\&=\tilde{U}_{\phi}(N_{\rm f1},N_{\rm c1},N_{\rm t1},N_{\rm f2},N_{\rm c2},N_{\rm t2})\cdot\tilde{U}_{\rm swap}(N_{\rm f0},N_{\rm c0},N_{\rm t0})\\&=\begin{bmatrix}1&0&0&0\\0&{\rm e}^{{\rm i}\phi_2}u_{22}&{\rm e}^{{\rm i}\phi_2}u_{23}&0\\0&{\rm e}^{{\rm i}\phi_1}u_{32}&{\rm e}^{{\rm i}\phi_1}u_{33}&0\\0&0&0&{\rm e}^{{\rm i}(\phi_1+\phi_2)}u_{44}\end{bmatrix}.\end{aligned}\tag{45}$$

For the ideal case, the operations above can be described by a matrix

$$\tilde{U}_{\rm ideal,iSWAP}=\begin{bmatrix}1&0&0&0\\0&0&-{\rm i}&0\\0&-{\rm i}&0&0\\0&0&0&1\end{bmatrix}.\tag{46}$$

Therefore, the selection of the values of $N_{\rm f0}$, $N_{\rm c0}$ and $N_{\rm t0}$ should make $|u_{22}|^2$ and $|u_{33}|^2$ as close to 0 as possible. The selection of the values of $N_{\rm f1},N_{\rm c1},N_{\rm t1},N_{\rm f2},N_{\rm c2}$ and $N_{\rm t2}$ for $\tilde{U}_{\phi}$ should make ${\rm e}^{{\rm i}\phi_2}u_{23}=-{\rm i}$, ${\rm e}^{{\rm i}\phi_1}u_{32}=-{\rm i}$, ${\rm e}^{{\rm i}(\phi_1+\phi_2)}u_{44}=1$.

3. Simulation and discussion

3.1. Simulation method

The first task of the simulation is to ensure the effectiveness of circuit design of DFTQs, which means the responses of $i_{\rm p}(t)$ to the input SFQ pulses of DFTQs should be consistent with the prediction by Eq. (5). The transient simulations with circuits shown in Fig. 4 are performed in Keysight's Advanced Design System (ADS). The circuit model of an ideal Josephson junction for simulation is built as a symbolically defined device (SDD) in ADS based on Josephson equations.[24] This method has been elucidated in Ref. [25]. The SFQ pulses sent to ports P1–P4 are generated by 4 DC/SFQs, driven by time-dependent current sources $I_{\rm SA}$–$I_{\rm SD}$, respectively. P5 and P6 of the DFTQ are connected to the inductor $L_{\rm p}$, as described in the previous text.

For gate simulations, the circuit schematic diagram is shown in Fig. 3(a). The waveforms of $i_{\rm p1}(t)$ and $i_{\rm p2}(t)$ are extracted from the simulations of DFTQs with specific input SFQ pulses. Then the waveform data is imported to the Hamiltonian described by Eq. (21), which is encoded as a time-domain function in Python programs for solving the states of qubits. The function as the solver, mesolve(), is called from QuTip, a set of open-source Python software for simulating the dynamics of open quantum systems.[26,27] The state probabilities and phases of qubits can be calculated with the solutions of states, which can be used to analyze gate operation time and gate fidelities.

For the convenience of evaluating the precision of a DFTQ, one can define

$$r_{\rm c}=\Phi_{\rm c}/\Phi_0,\tag{47}$$

$$r_{\rm f}=\Phi_{\rm f}/\Phi_0\tag{48}$$

as the ratios of the increment units of the flux $\Phi_{\rm e}$ with coarse tuning and fine-tuning by DFTQ to the flux quantum Φ_0, respectively. $r_{\rm f}$ should be small enough for high precision. Meanwhile, to obtain fast operation, $r_{\rm c}$ should be big enough for $i_{\rm p}(t)$ to quickly reach the target value $i_{\rm target}$. The ratio of the two increment units can be defined as

$$r_{\rm cf}=\Phi_{\rm c}/\Phi_{\rm f}.\tag{49}$$

The three ratios should be set properly when the DFTQ is designed. In the following simulations, the parameters above are $r_{\rm c}=0.032$, $r_{\rm f}=0.001$ and $r_{\rm cf}=32$.

3.2. Simulation of a single DFTQ

The circuit parameters for testing DFTQ are shown in Table 1. Simulation results for the case of $\Delta t=1$ ns, $N_{\rm c}=2$, $N_{\rm f}=2$ and $N_{\rm t}=10$ are shown in Fig. 5. With triangular current excitation pulses from current sources, $I_{\rm SA}$–$I_{\rm SD}$, as inputs, the four DC/SFQs in Fig. 4 can generate SFQ pulses with different Δt, $N_{\rm c}$, $N_{\rm f}$ and $N_{\rm t}$. The curve of $i_{\rm p}(t)$ is similar to that of $i_{\rm z}(t)$, which increases or decreases step by step when an SFQ pulse is input to the DFTQ and maintains at a constant when no SFQ pulse is input.

To verify the effectiveness of Eq. (5), simulations with combinations of $N_{\rm t}=10$, $\Delta t=1$ ns and different values of $N_{\rm c}$ and $N_{\rm f}$ are carried out to see the differences between the simulation results of the $i_{\rm p}(t)$ and the predictions of Eq. (5), which are shown in Table 2. The values of $\Delta i_{\rm c}$ and $\Delta i_{\rm f}$ in the simulations are a little smaller than those of the predictions. It can be seen that the relative errors of simulation results to the predictions are all around -2%, which means Eq. (5) can basically predict the output signal $i_{\rm p}(t)$ of the DFTQ. For designing a DFTQ, Eq. (5) can be helpful for determining the rough ranges of the values of the inductors listed in Table 1. In the following simulations of the Z gate and the iSWAP gate, the value of $L_{\rm p}$ is revised as 220.72 pH to eliminate the relative errors.

Table 1. DFTQ circuit parameters for DFTQ simulation.

Parameter	Value (μA)	Parameter	Value (Ω)	Parameter	Value (pH)	Parameter	Value (pH)
J_1	80	R_1	0.766	L_{11}	200.00	M_1	147.13
J_2	80	R_2	0.766	L_{12}	169.11	M_2	459.77
J_3	80	R_3	0.766	L_{31}	200.00	$L_{\rm p}$*	229.89
J_4	80	R_4	0.766	L_{32}	169.11	M	20.00

*Note: $L_{\rm p}$ is revised as 220.72 pH for the following Z gate and iSWAP gate simulations.

Table 2. Differences between simulation results and predictions of Eq. (5) for $i_p(t)$.

Parameters		Simulation results (μA)			Predictions (μA)	Relative errors (%)		
N_c	N_f	Δi_c in avg.	Δi_f in avg.	max $i_p(t)$	max $i_p(t)$	for Δi_c	for Δi_f	for max $i_p(t)$
1	0	3.2430	–	3.2430	3.3085	−1.9808	–	−1.9808
0	1	–	0.10130	0.10130	0.10339	–	−2.0231	−2.0231
1	1	3.2427	0.10130	3.3440	3.4119	−1.9898	−2.0231	−1.9908
2	0	3.2425	–	6.4850	6.6171	−1.9959	–	−1.9959
0	2	–	0.10135	0.20270	0.20678	–	−1.9747	−1.9747
2	1	3.2429	0.10135	6.5870	6.7205	−1.9853	−2.0231	−1.9859
1	2	3.2423	0.10135	3.4550	3.5153	−2.0019	−1.9747	−2.0003
2	2	3.2427	0.10135	6.6880	6.8239	−1.9913	−1.9747	−1.9908
3	0	3.2427	–	9.7280	9.9256	−1.9908	–	−1.9908
0	3	–	0.10133	0.30400	0.31018	–	−1.9909	−1.9908
3	1	3.2426	0.10130	9.8290	10.029	−1.9939	−2.0231	−1.9942
1	3	3.2430	0.10133	3.5470	3.6187	−1.9808	−1.9909	−1.9816
3	2	3.2424	0.10135	9.9300	10.132	−1.9979	−1.9747	−1.9974
2	3	3.2425	0.10133	6.7890	6.9272	−1.9959	−1.9909	−1.9957
3	3	3.2420	0.10133	10.030	10.236	−2.0110	−1.9909	−2.0104

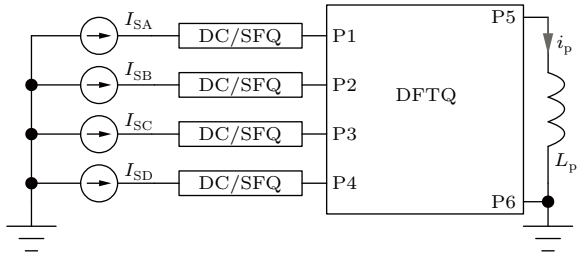


Fig. 4. Simulation circuits for testing DFTQ. SFQ pulses generated from DC/SFQs are input to ports P1–P4 of the DFTQ. P5 and P6 are connected to the inductor L_p. DC/SFQs are driven by the current sources I_{SA}, I_{SB}, I_{SC} and I_{SD}.

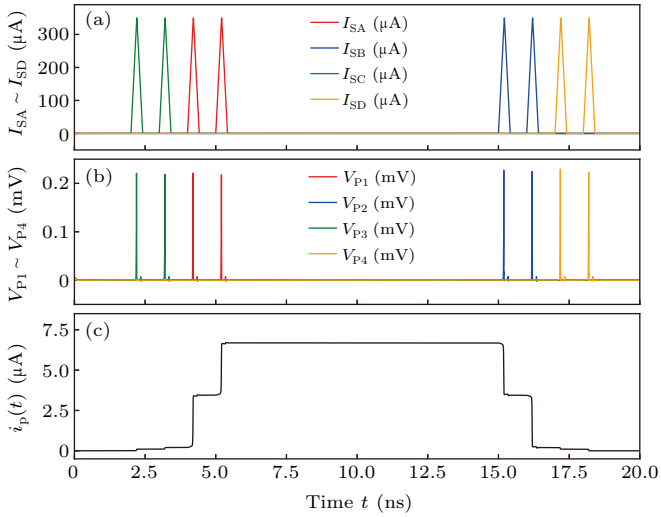


Fig. 5. DFTQ simulation results. (a) Input signals to DC/SFQs from current sources. (b) Input SFQ pulses generated from DC/SFQs, with $\Delta t = 1$ ns, $N_c = 2$, $N_f = 2$, $N_t = 10$ and $i_{ref} = 0$ A. (c) Inductor loop current $i_p(t)$, with a curve similar to that in Fig. 2(b).

3.3. Simulation of Z gate

The Z gate simulation here is only for the Z gate performed to qubit 1. The simulation for the Z gate performed to qubit 2 can be carried out in a similar way. The parameters of the two DFTQs in Fig. 3(b) are set according to Table 1. The qubit parameters for the Z gate simulation are shown in Table 3, with idle frequencies $f_1 = \omega_1/(2\pi) = 5.957$ GHz and $f_2 = \omega_2/(2\pi) = 5.359$ GHz for qubit 1 and qubit 2, respectively, which are selected for gaining a sufficiently high gate fidelity. These frequencies can be realized by designing bare frequencies of qubits or setting the reference levels i_{ref1} and i_{ref2} of DFTQs. E_{J11}, E_{J12}, E_{J21} and E_{J22} are the Josephson energies of Josephson junctions J_{11}, J_{12}, J_{21} and J_{22}, respectively. E_{C1} and E_{C2} are the charging energies of capacitors C_1 and C_2. The units of these parameters have been transformed to GHz or MHz by dividing them by Plank constant h or 2π.

Table 3. Qubit parameters for Z gate and iSWAP gate simulations.

Parameter	Value (GHz)	Parameter	Value (MHz)	Parameter	Value (MHz)
E_{J11}/h	10	E_{C1}/h	240	$\alpha_1/(2\pi)$	−240
E_{J12}/h	10	E_{C2}/h	240	$\alpha_2/(2\pi)$	−240
E_{J21}/h	8.163	f_1	5957	$g/(2\pi)$	6.25
E_{J22}/h	8.163	f_2	5359		

To determine the waveform parameters of $i_{p1}(t)$ and $i_{p2}(t)$ including N_{c1}, N_{f1}, N_{t1}, N_{c2}, N_{f2}, N_{t2} and Δt, the unitary matrix $\tilde{U}_{DFTQ,Z1}$ of Z gates with different waveform parameters are first calculated according to Eqs. (30)–(32) and (20). Then the corresponding final state fidelities are obtained by[28]

$$\mathcal{F}\left(\tilde{U}_T, W, N\right) = \frac{1}{2} + \frac{1}{2N}\mathrm{Re}\left\{\mathrm{Tr}\left(W^\dagger \tilde{U}_T\right)\right\}, \tag{50}$$

where W is the ideal gate, $\tilde{U}_T$ is the gate performed, and N is the dimension of these matrices. To calculate the final state fidelity of the Z gate to qubit 1, there should be $W = \tilde{U}_{ideal,Z1}$, $\tilde{U}_T = \tilde{U}_{DFTQ,Z1}$ and $N = 4$. The combinations of parameters of waveforms with gate fidelities over the threshold for error correction can be collected and put into a set. Then the combinations with short operation time and few Josephson junction switching times are selected for waveform generation.

The waveform parameters of $i_{p1}(t)$ and $i_{p2}(t)$ for this simulation are $N_{c1}=4$, $N_{f1}=2$, $N_{t1}=3$, $N_{c2}=N_{f2}=N_{t2}=0$ and $\Delta t=0.4$ ns.

The results of Z gate simulation are shown in Fig. 6. The final state fidelity is 99.948%, with the total gate operation time $T_Z=5.2$ ns. When qubit 1 is idle, the qubit frequency $f_{q1}(t)=\omega_{q1}(t)/(2\pi)=f_1=5.957$ GHz. When $\Phi_{e1}(t)$ turns to the maximum ($\Phi_{e1,max}=4\Phi_c+2\Phi_f=0.13\Phi_0$), its frequency $f_{q1}(t)$ turns to the minimum, 5.696 GHz. The maximum external flux $\Phi_{e1,max}$ corresponds to $i_{p1}(t)=13.439$ μA. The variation of $f_{q1}(t)$ increases when $n_c(t)$ and $n_f(t)$ increase, so the phase of qubit 1 (φ_1), changes faster with bigger $i_{p1}(t)$. Considering the lowest three energy levels of each qubit, the initial state of the two-qubit system is

$$\begin{aligned}\Psi_{init} &= \frac{1}{2}(|00\rangle+|01\rangle+|10\rangle+|11\rangle)\\ &= \left[0.5\ 0.5\ 0\ 0.5\ 0.5\ 0\ 0\ 0\right]^{\mathrm{T}}.\end{aligned}\tag{51}$$

The ideal end state should be

$$\begin{aligned}\Psi_{end,ideal} &= \frac{1}{2}(|00\rangle+|01\rangle-|10\rangle-|11\rangle)\\ &= \left[0.5\ 0.5\ 0\ -0.5\ -0.5\ 0\ 0\ 0\right]^{\mathrm{T}}.\end{aligned}\tag{52}$$

With the Z gate described above, the end state computed by simulation is

$$\Psi_{end,sim}=\begin{bmatrix}0.50127944\\ 0.50377703+0.00134198\mathrm{i}\\ -0.00885927-0.00669337\mathrm{i}\\ -0.49622297+0.02807619\mathrm{i}\\ -0.49708356+0.02181554\mathrm{i}\\ 0\\ -0.00502104-0.01355847\mathrm{i}\\ 0\\ 0\end{bmatrix}.\tag{53}$$

The standard quantum process tomography[29,30] is performed in order to fully understand the process of the Z gate to qubit 1. The operation of a quantum gate V (like Z, iSWAP or other gates) can be represented by the bases $\tilde{E}_m$ of the operator

$$V=\sum_m e_m\tilde{E}_m,\tag{54}$$

where $\tilde{E}_m$ belongs to a set of tenser products of two Pauli operators, that is, $\tilde{E}_m\in\{P_i\otimes P_j\}$ $(P_i,P_j\in\{I,X,Y,Z\})$. The end density matrix from the evolution of the initial density matrix ρ in the process ε can be defined by

$$\varepsilon(\rho)=V\rho V^{\dagger}.\tag{55}$$

Considering the two equations above, the process ε can be expressed by[29,30]

$$\varepsilon(\rho)=\sum_{mn}\chi_{mn}\tilde{E}_m\rho\tilde{E}_n^{\dagger},\tag{56}$$

where $\chi_{mn}=e_me_n^*$ is the element at the m^{th} line and n^{th} column of a matrix χ. It is called the process matrix, which fully characterizes the operation to the initial density matrices of qubits, so the target of process tomography is to obtain χ. The process fidelity $\mathcal{F}_p$ is obtained with the trace of the product of χ and the ideal process matrix χ_{ideal}:[31]

$$\mathcal{F}_p=\mathrm{tr}(\chi_{ideal}\chi).\tag{57}$$

Then the gate fidelity $\mathcal{F}_g$ independent of the initial states can be calculated with[31–33]

$$\mathcal{F}_g=\frac{1+d\mathcal{F}_p}{1+d},\tag{58}$$

where $d=2^N$ is the dimension of Hilbert space of the N-qubit system. For two-qubit systems, $d=2^2=4$.

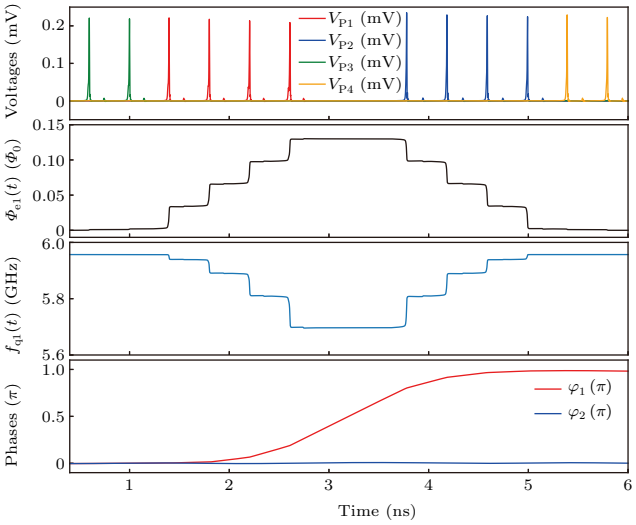


Fig. 6. Simulation results of the Z gate for qubit 1. The waveform parameters are $N_{c1}=4$, $N_{f1}=2$, $N_{t1}=3$, $N_{c2}=0$, $N_{f2}=0$, $N_{t2}=0$ and $\Delta t=0.4$ ns. The final state fidelity is 99.948% with the total gate operation time T_Z of 5.2 ns. The maximum external flux is $\Phi_{e1,max}=4\Phi_c+2\Phi_f=0.13\Phi_0$. (a) SFQ pulses generated from DC/SFQs. (b) The external flux $\Phi_{e1}(t)$ of qubit 1. (c) The bare frequency of qubit 1, $f_{q1}(t)$. When qubit 1 is idle, $f_{q1}(t)=f_1=5.957$ GHz. When $\Phi_{e1}(t)$ turns to the maximum (corresponding to $i_{p1}(t)=13.439$ μA), its frequency turns to the minimum, 5.696 GHz. (d) The phases of qubit 1 and qubit 2. When the Z gate for qubit 1 is performed, its phase is changed faster with bigger $i_{p1}(t)$ and the phase of qubit 2 remains unchanged.

The ideal process matrix χ_{ideal}^{Z1} of the Z gate to qubit 1 and its process matrix χ^{Z1} from simulation are plotted in Figs. 7(a)–7(d). The line numbers and column numbers on the axes of all subfigures in Fig. 7 are replaced by labels of corresponding basis $\tilde{E}_m$. For example, the line number 1 and the column number 1 are replaced by the label "II", which represents the basis $\tilde{E}_1=I\otimes I$. For the ideal Z gate, there is only one non-zero element at the "ZI" line and the "ZI" column in the real part of χ_{ideal}^{Z1}, which is consistent with the unitary operator $\tilde{U}_{ideal,Z1}=Z\otimes I$. However, χ^{Z1} has non-zero elements corresponding to the bases with line or column labels "XX", "YY" in the real part and "II", "ZZ" in the imaginary part. This leads to the imperfect process fidelity $\mathcal{F}_p^{Z1}$ of the Z gate,

99.918%, and thus the gate fidelity $\mathcal{F}_{\rm g}^{Z1}$ is 99.935% according to Eqs. (57) and (58). To show the difference more significantly, Figs. 7(e) and 7(f) present the real and imaginary parts of the difference between the two process matrices.

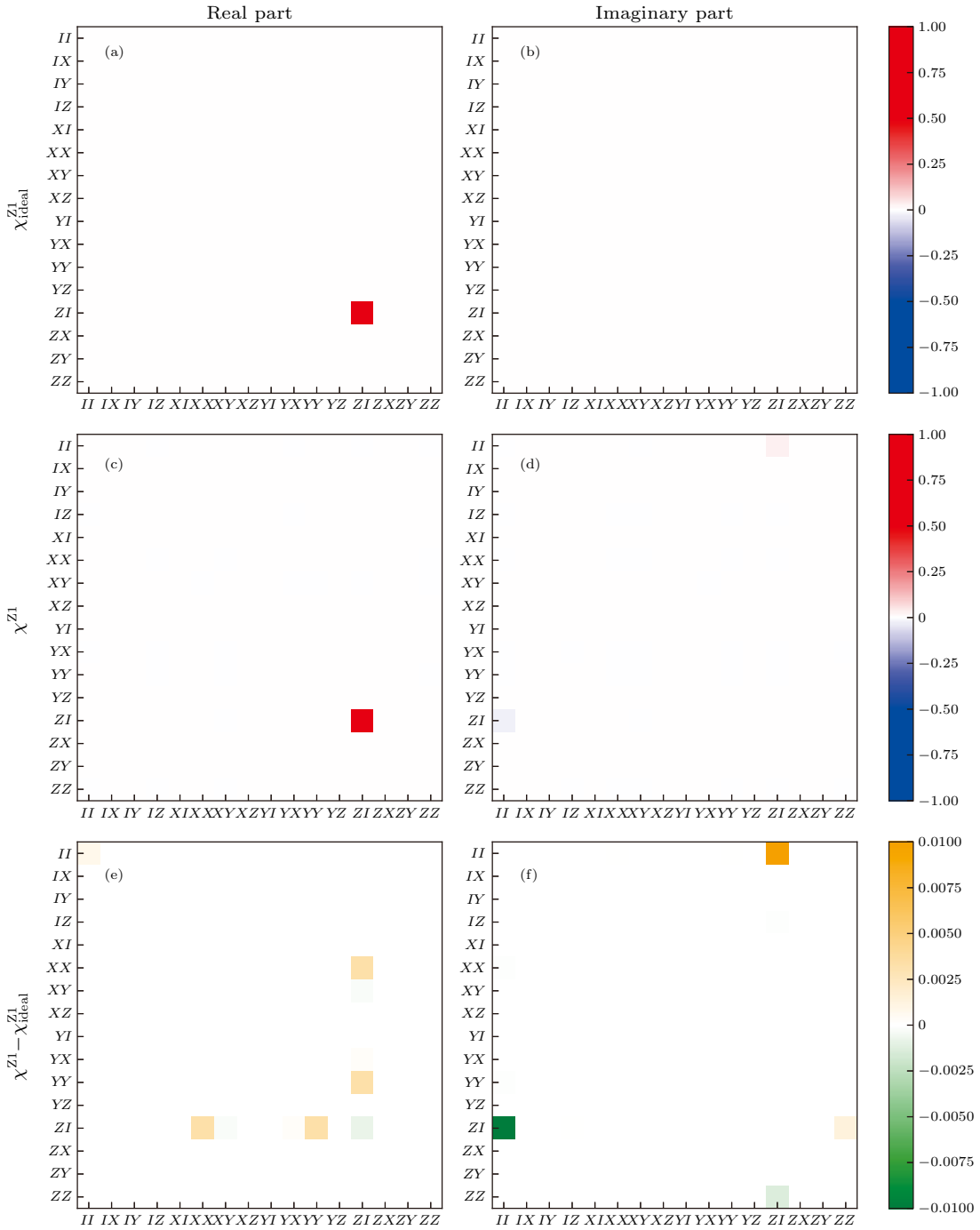


Fig. 7. Results of quantum process tomography to the Z gate for qubit 1 of the two-qubit system. (a) and (b) The real and imaginary parts of the ideal process matrix $\chi^{Z1}_{\rm ideal}$ of the Z gate, respectively. (c) and (d) The real and imaginary parts of process matrix χ^{Z1} from the Z gate simulation. (e) and (f) The real part and imaginary parts of the difference between the two process matrices, $\chi^{Z1}-\chi^{Z1}_{\rm ideal}$. The process fidelity $\mathcal{F}_{\rm p}^{Z1}$ of the Z gate is 99.918% and thus the gate fidelity $\mathcal{F}_{\rm g}^{Z1}$ calculated with the process matrix is 99.935%.

3.4. Simulation of iSWAP gate

The iSWAP gate simulations are performed for two specific initial states. The parameters of the DFTQs and qubits are set as the same values of the Z gate simulation. Before running the program for simulation, the waveform parameters of $i_{\rm p1}(t)$ and $i_{\rm p2}(t)$ including $N_{\rm c0}$, $N_{\rm f0}$, $N_{\rm t0}$, $N_{\rm c1}$, $N_{\rm f1}$, $N_{\rm t1}$, $N_{\rm c2}$, $N_{\rm f2}$, $N_{\rm t2}$ and Δt shown in Fig. 3 should be determined. In order to tune the frequency of qubit 1, $f_{\rm q1}(t)$, to be the same as the bare frequency of qubit 2, f_2, there should be $N_{\rm c0}=6$ and $N_{\rm f0}=4$. Then, because the coupling strength is $g/(2\pi)=6.25$ MHz, with $N_{\rm t0}=100$ and $\Delta t=0.4$ ns, there should be $gN_{\rm t0}\Delta t=\pi/2$,[1] which means $N_{\rm t0}\Delta t=40$ ns is spent for swapping the states of qubits. After swapping states, the phases of qubits may be different from $-\pi/2+2n\pi$

($n \in \mathbb{Z}$), which corresponds to the probability amplitude $-\mathrm{i}$, so a gate for adjusting the phases, $\tilde{U}_{\varphi}(N_{c1}, N_{f1}, N_{t1}, N_{c2}, N_{f2}, N_{t2})$ is required. To get the right phases $-\pi/2 + 2n\pi$, the simulation of swapping states is carried out and the phases at the end of swapping, $\varphi_{1,\mathrm{swap}}$ and $\varphi_{2,\mathrm{swap}}$, are calculated with the end state of swapping before $\tilde{U}_{\phi}$. Then the combinations of values of $N_{c1}, N_{f1}, N_{t1}, N_{c2}, N_{f2}$ and N_{t2} are searched for the proper one to eliminate the differences between the phases and $-\pi/2$, so that $\varphi_1 = \phi_1 + \varphi_{1,\mathrm{swap}} = -\pi/2 + 2n_1\pi$ and $\varphi_2 = \phi_2 + \varphi_{2,\mathrm{swap}} = -\pi/2 + 2n_2\pi$ ($n_1, n_2 \in \mathbb{Z}$). For this work, $N_{c1} = 2, N_{f1} = 1, N_{t1} = 6, N_{c2} = 3, N_{f2} = 0$ and $N_{t2} = 2$. At last, the formal iSWAP gate simulations with all the parameters mentioned above are performed.

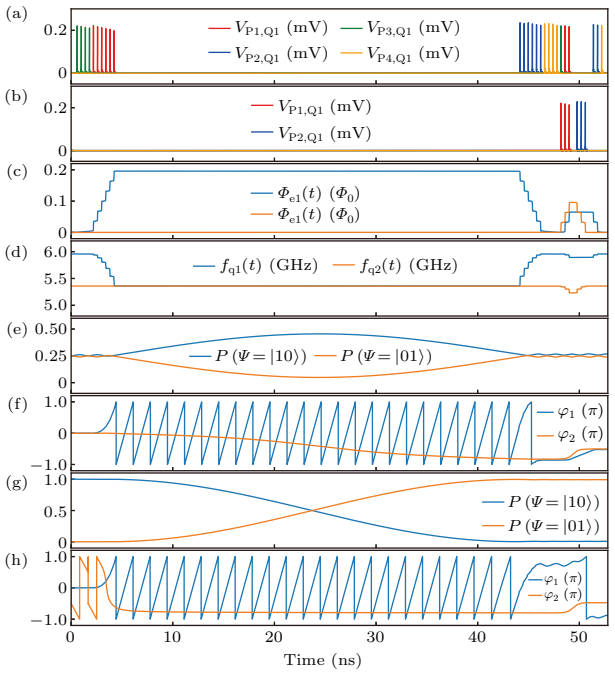


Fig. 8. Simulation results of iSWAP gates. The waveform parameters are $N_{c0} = 6, N_{f0} = 4, N_{t0} = 100, N_{c1} = 2, N_{f1} = 1, N_{t1} = 6, N_{c2} = 3, N_{f2} = 0, N_{t2} = 2$ and $\Delta t = 0.4$ ns. For the initial state $(|00\rangle + |01\rangle + |10\rangle + |11\rangle)/2$, the final state fidelity is 99.843%. For the initial state $|10\rangle$, the final state fidelity is 99.692%. The total operation time is 51.6 ns. (a) The SFQ pulses input to DFTQ 1 for qubit 1. (b) The SFQ pulses input to DFTQ 2 for qubit 2. (c) The external fluxes $\Phi_{e1}(t)$ and $\Phi_{e2}(t)$ of qubit 1 and qubit 2, respectively. (d) The bare frequencies $f_{q1}(t)$ and $f_{q2}(t)$ of qubit 1 and qubit 2, respectively. (e) The probabilities of states $|10\rangle$ and $|01\rangle$ for the initial state $(|00\rangle + |01\rangle + |10\rangle + |11\rangle)/2$. (f) The phases φ_1 and φ_2 of qubit 1 and qubit 2 for the initial state $(|00\rangle + |01\rangle + |10\rangle + |11\rangle)/2$, respectively. (g) The probabilities of states $|10\rangle$ and $|01\rangle$ for the initial state $|01\rangle$. (h) The phases φ_1 and φ_2 of qubit 1 and qubit 2 for the initial state $|01\rangle$, respectively.

Figure 8 presents the simulation results of iSWAP gates. Figures 8(a) and 8(b) are SFQ pulses input to DFTQs. Figure 8(c) shows the external fluxes Φ_{e1} and Φ_{e2}, which are similar to the waveforms of inductor loop currents shown in Fig. 3. In Fig. 8(d), the bare frequency of qubit 1, $f_{q1}(t)$, is changed to the bare frequency of qubit 2, $f_{q2}(t)$ ($f_{q2}(t) = \omega_{q2}(t)/(2\pi)$), when the states are swapping, then the phases of qubits are adjusted with their small variation. Figures 8(e) and 8(f) show the probabilities of $|10\rangle$ and $|01\rangle$ for different initial states,

$$\begin{aligned}\Psi_{\mathrm{init1}} &= \frac{1}{2}(|00\rangle + |01\rangle + |10\rangle + |11\rangle) \\ &= [0.5\ 0.5\ 0\ 0.5\ 0.5\ 0\ 0\ 0\ 0]^{\mathrm{T}}, \end{aligned} \tag{59}$$

$$\Psi_{\mathrm{init2}} = |10\rangle = [0\ 0\ 0\ 1\ 0\ 0\ 0\ 0\ 0]^{\mathrm{T}}, \tag{60}$$

respectively. The corresponding ideal end states are

$$\begin{aligned}\Psi_{\mathrm{end1,ideal}} &= \frac{1}{2}(|00\rangle - \mathrm{i}|01\rangle - \mathrm{i}|10\rangle + |11\rangle) \\ &= [0.5\ \ -0.5\mathrm{i}\ \ 0\ \ -0.5\mathrm{i}\ \ 0.5\ \ 0\ \ 0\ \ 0\ \ 0]^{\mathrm{T}}, \end{aligned} \tag{61}$$

$$\Psi_{\mathrm{end2,ideal}} = -\mathrm{i}|01\rangle = [0\ \ -\mathrm{i}\ \ 0\ \ 0\ \ 0\ \ 0\ \ 0\ \ 0\ \ 0]^{\mathrm{T}}. \tag{62}$$

The corresponding end states in the simulation results are

$$\Psi_{\mathrm{end1,sim}} = \begin{bmatrix} 0.51021949 \\ -0.00604606 - 0.48907264\mathrm{i} \\ -0.01499452 + 0.0009786\mathrm{i} \\ -0.03236018 - 0.51575929\mathrm{i} \\ 0.48038327 - 0.03684263\mathrm{i} \\ 0 \\ 0.03057866 - 0.01031202\mathrm{i} \\ 0 \\ 0 \end{bmatrix}, \tag{63}$$

$$\Psi_{\mathrm{end2,sim}} = \begin{bmatrix} 0 \\ 0.08013727 - 0.99369771\mathrm{i} \\ 0 \\ -0.07257209 - 0.02960006\mathrm{i} \\ 0 \\ 0 \\ 0 \\ 0 \\ 0 \end{bmatrix}. \tag{64}$$

Figures 8(g) and 8(h) show the phases of qubit 1 and qubit 2 for the two different initial states. The total gate operation time is $T_{\mathrm{iSWAP}} = 51.6$ ns with gate fidelities 99.843% for Ψ_{init1} and 99.692% for Ψ_{init2}.

The standard quantum process tomography for the iSWAP gate is also performed. The ideal process matrix $\chi_{\mathrm{ideal}}^{\mathrm{iSWAP}}$ of the iSWAP gate and its process matrix χ^{iSWAP} from simulation are plotted in Figs. 9(a)–9(d). The process matrix χ^{iSWAP} has non-zero elements corresponding to the bases with labels including "*IZ*", "*XY*", "*YX*" and "*ZI*" in both real and imaginary parts, which are not required for gate operation and lead to the imperfect process fidelity $\mathcal{F}_{\mathrm{p}}^{\mathrm{iSWAP}}$ of the iSWAP gate, 99.596% and the gate fidelity $\mathcal{F}_{\mathrm{g}}^{\mathrm{iSWAP}} = 99.676\%$ according to Eqs. (57) and (58). The elements corresponding to "*IZ*" in the matrix of the difference of χ^{iSWAP} and $\chi_{\mathrm{ideal}}^{\mathrm{iSWAP}}$ in Figs. 9(e) and 9(f) are more prominent than other not-required elements, which means the gate error caused by control error mainly comes from imperfect phase adjustment to qubit 2 after state swapping. Apart from the control error and decoherence, leakage of energy to non-computation-basis levels also leads to gate error. For a system consisting of qubit

A and B coupled with a capacitor, the leakage from $|11\rangle$ to $(|20\rangle+|02\rangle)/\sqrt{2}$ occurs when the transition frequency of the second and the third energy level of qubit A, f_{21}^{A}, sweeps by the transition frequency of the first and the second energy level of the other qubit B, f_{10}^{B}.[34] Here, in the simulation for the initial state $(|00\rangle+|01\rangle+|10\rangle+|11\rangle)/2$, there is leakage of a small part of energy from state $|11\rangle$ to $(|20\rangle+|02\rangle)/\sqrt{2}$, which can be found with the non-zero elements at the third and the seventh lines (corresponding to $|02\rangle$ and $|20\rangle$) of $\Psi_{\mathrm{end1,sim}}$ in Eq. (63). Leakage can also be found in the Z gate performed to qubit 1 with the elements at the third and the seventh lines of $\Psi_{\mathrm{end,sim}}$ in Eq. (53), which is weaker than that of the iSWAP gate because there is still a detuned amount of f_{21}^{A} and f_{10}^{B} of $5.456-5.359=0.097$ GHz for the Z gate. Leakage can be suppressed by synchronizing the entangling parameters (hold time, overshoot frequencies and interaction frequencies), leakage channels, and the weakly frequency-dependent interqubit coupling.[34]

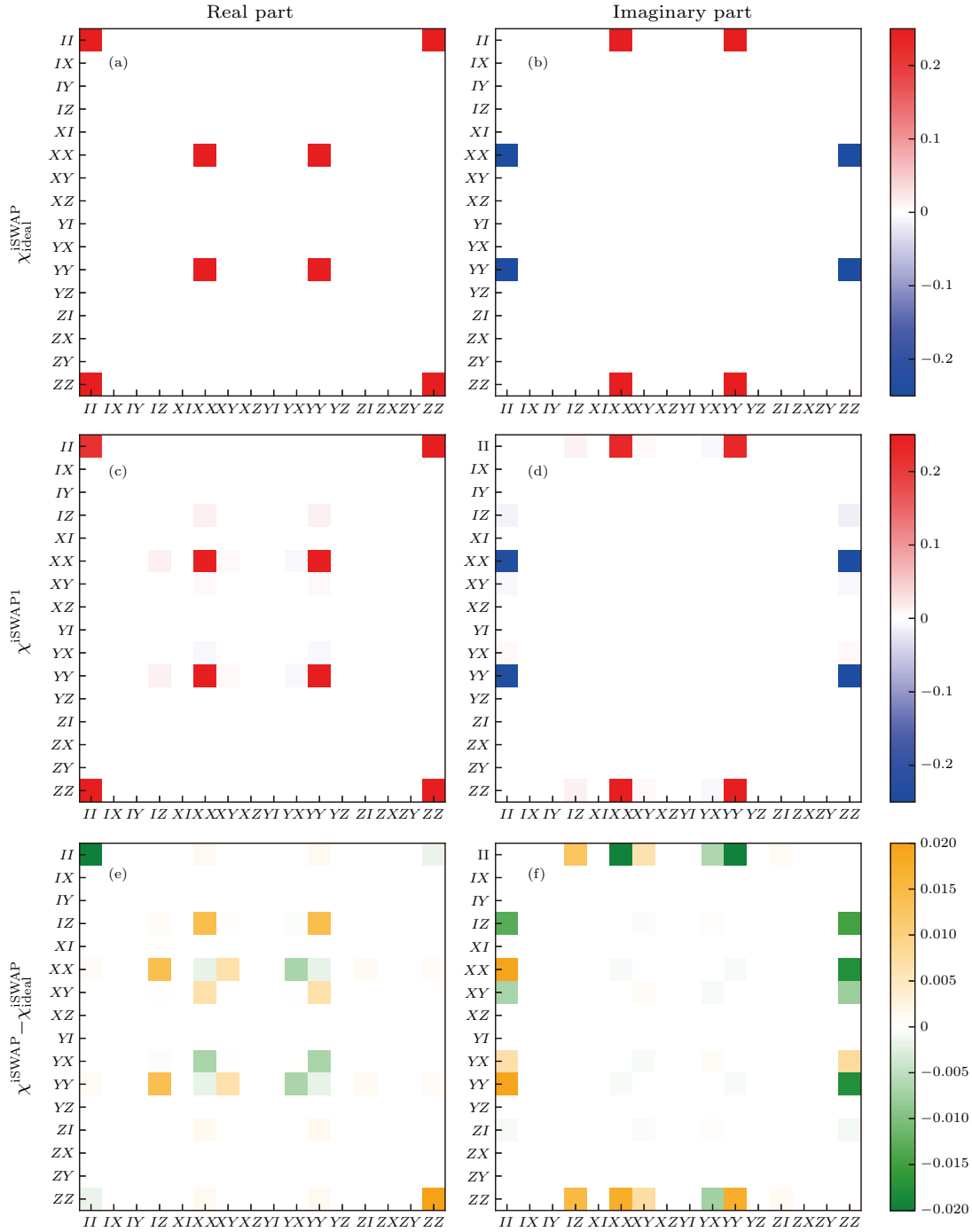


Fig. 9. Results of quantum process tomography to the iSWAP gate. (a) and (b) The real and imaginary parts of the ideal process matrix $\chi_{\mathrm{ideal}}^{\mathrm{iSWAP}}$ of the iSWAP gate. (c) and (d) The real and imaginary parts of the process matrix χ^{iSWAP} from iSWAP gate simulation. (e) and (f) The real and imaginary parts of the difference between the two process matrices, $\chi^{\mathrm{iSWAP}}-\chi_{\mathrm{ideal}}^{\mathrm{iSWAP}}$. The process fidelity $\mathcal{F}_{\mathrm{p}}^{\mathrm{iSWAP}}$ of the iSWAP gate is 99.596% and thus the gate fidelity $\mathcal{F}_{\mathrm{g}}^{\mathrm{iSWAP}}$ calculated with the process matrix is 99.676%.

4. Summary

In order to realize RSFQ-based flux tuning for flux-tunable transmon qubits, a circuit called digital flux tuner for qubits (DFTQ) is proposed. This work analyzed the circuit schematic diagram of the DFTQ consisting of a fine-tuning unit and a coarse tuning unit, and derived the formula predicting the inductor loop current for tuning the flux with SFQ pulses as inputs. The control model of Z control to a two-qubit system is established for Z gate and iSWAP gate simulations. The method of simulations based on ADS and QuTip for a single DFTQ, a Z gate and an iSWAP gate by DFTQs is introduced. Results show that the predictive values of the inductor loop current of the DFTQ are different from simulation results with relative error of about -2%. The final state fidelity in the Z gate simulation is 99.948% with the total operation time of 5.2 ns. The final state fidelities in the iSWAP gate simulations are 99.843% and 99.692% for two different initial states, with the total operation time of 51.6 ns. The standard quantum process tomography for the Z gate and the iSWAP gate is performed and the corresponding gate fidelities are 99.935% and 99.676%. Gate errors are mainly caused by the control error of qubit phase adjustment and the leakage to non-computation-basis energy levels. In conclusion, the DFTQ is able to perform Z gates and iSWAP gates for flux-tunable transmon qubits with pure SFQ pulse sequences as inputs, which means the DFTQ has potential to be a crucial part of QCI for the Z control of qubits.

Appendix A: Derivation of formula for inductor loop current

According to Kirchhoff's voltage law, the relationships between the voltages of nodes A, B, C and D in Fig. 1 are

$$V_{\mathrm{A}}(t')-V_{\mathrm{B}}(t')=L_{11}\frac{\mathrm{d}i_1(t')}{\mathrm{d}t'}-M_1\frac{\mathrm{d}i_{\mathrm{p}}(t')}{\mathrm{d}t'}, \tag{A1}$$

$$V_{\mathrm{C}}(t')-V_{\mathrm{D}}(t')=L_{31}\frac{\mathrm{d}i_2(t')}{\mathrm{d}t'}-M_2\frac{\mathrm{d}i_{\mathrm{p}}(t')}{\mathrm{d}t'}. \tag{A2}$$

When P5 and P6 are connected to the inductor L_{p}, there is

$$0=\left(L_{12}+L_{32}+L_{\mathrm{p}}\right)\frac{\mathrm{d}i_{\mathrm{p}}(t')}{\mathrm{d}t'}-M_1\frac{\mathrm{d}i_1(t')}{\mathrm{d}t'}-M_2\frac{\mathrm{d}i_2(t')}{\mathrm{d}t'}. \tag{A3}$$

With the zero initial condition, integrating both sides of Eqs. (A1)–(A3) with 0 as lower bound and time t as upper bound yields

$$\Phi_{\mathrm{A}}(t)-\Phi_{\mathrm{B}}(t)=L_{11}i_1(t)-M_1i_{\mathrm{p}}(t), \tag{A4}$$

$$\Phi_{\mathrm{C}}(t)-\Phi_{\mathrm{D}}(t)=L_{31}i_2(t)-M_2i_{\mathrm{p}}(t), \tag{A5}$$

$$0=L_{\Sigma}i_{\mathrm{p}}(t)-M_1i_1(t)-M_2i_2(t), \tag{A6}$$

where

$$\Phi_{\mathrm{A}}(t)=\int_0^t V_{\mathrm{A}}(t')\mathrm{d}t', \tag{A7}$$

$$\Phi_{\mathrm{B}}(t)=\int_0^t V_{\mathrm{B}}(t')\mathrm{d}t', \tag{A8}$$

$$\Phi_{\mathrm{C}}(t)=\int_0^t V_{\mathrm{C}}(t')\mathrm{d}t', \tag{A9}$$

$$\Phi_{\mathrm{D}}(t)=\int_0^t V_{\mathrm{D}}(t')\mathrm{d}t', \tag{A10}$$

$$L_{\Sigma}=L_{12}+L_{32}+L_{\mathrm{p}}. \tag{A11}$$

Then, let

$$\boldsymbol{\Phi}(t)=\begin{bmatrix}\Phi_{\mathrm{A}}(t)-\Phi_{\mathrm{B}}(t)\\ \Phi_{\mathrm{C}}(t)-\Phi_{\mathrm{D}}(t)\\ 0\end{bmatrix}, \tag{A12}$$

$$\boldsymbol{i}(t)=\begin{bmatrix}i_1(t)\\ i_2(t)\\ i_{\mathrm{p}}(t)\end{bmatrix}, \tag{A13}$$

$$\boldsymbol{L}=\begin{bmatrix}L_{11} & 0 & -M_1\\ 0 & L_{31} & -M_2\\ -M_1 & -M_2 & L_{\Sigma}\end{bmatrix}, \tag{A14}$$

so that accroding to Eqs. (A4)–(A6) we have

$$\boldsymbol{\Phi}(t)=\boldsymbol{L}\boldsymbol{i}(t). \tag{A15}$$

To get $\boldsymbol{i}(t)$, we have

$$\boldsymbol{i}(t)=\boldsymbol{L}^{-1}\boldsymbol{\Phi}(t), \tag{A16}$$

where

$$\boldsymbol{L}^{-1}=\begin{bmatrix}L_{31}L_{\Sigma}-M_2^2 & M_1M_2 & L_{31}M_1\\ M_1M_2 & L_{11}L_{\Sigma}-M_1^2 & L_{11}M_2\\ M_1L_{31} & L_{11}M_2 & L_{11}L_{31}\end{bmatrix}\times\frac{1}{L_{11}L_{31}L_{\Sigma}-M_2^2L_{11}-M_1^2L_{31}}. \tag{A17}$$

Therefore, with Eqs. (A12), (A13), (A16) and (A17), the inductor loop current $i_{\mathrm{p}}(t)$ is obtained as

$$i_{\mathrm{p}}(t)=\frac{M_1L_{31}\left[\Phi_{\mathrm{A}}(t)-\Phi_{\mathrm{B}}(t)\right]+M_2L_{11}\left[\Phi_{\mathrm{C}}(t)-\Phi_{\mathrm{D}}(t)\right]}{L_{11}L_{31}L_{\Sigma}-M_2^2L_{11}-M_1^2L_{31}}. \tag{A18}$$

Acknowledgment

The authors acknowledge the discussion with Hao Li, Yongcheng He, Genting Dai, Liangliang Yang, Xinyu Wu, Qing Yu, Mingjun Cheng, and Guodong Chen about the methodology of the article.

References

[1] Krantz P, Kjaergaard M, Yan F, Orlando T P, Gustavsson S and Oliver W D 2019 *Appl. Phys. Rev.* **6** 021318
[2] Bardin J C, Slichter D H and Reilly D J 2021 *IEEE J. Microwaves* **1** 403
[3] Google Quantum A I 2023 *Nature* **614** 676
[4] Gong M, Wang S, Zha C, *et al.* 2021 *Science* **372** 948

[5] Arute F, Arya K, Babbush R, *et al*. 2019 *Nature* **574** 505
[6] Xue X, Patra B, van Dijk J P G, *et al*. 2021 *Nature* **593** 205
[7] Likharev K K and Semenov V K 1991 *IEEE T. Appl. Supercon.* **1** 3
[8] Opremcak A, Pechenezhskiy I V, Howington C, *et al*. 2018 *Science* **361** 1239
[9] Liu C H, Ballard A, Olaya D, *et al*. 2023 *PRX Quantum* **4** 030310
[10] McDermott R, Vavilov M G, Plourde B L T, Wilhelm F K, Liebermann P J, Mukhanov O A and Ohki T A 2018 *Quantum Sci. Technol.* **3** 024004
[11] McDermott R and Vavilov M G 2014 *Phys. Rev. Appl.* **2** 014007
[12] Vozhakov V, Bastrakova M, Klenov N, Satanin A and Soloviev I 2023 *Quantum Sci. Technol.* **8** 035024
[13] Liu K, Wang Y, Ji B, Gao W, Lin Z and Wang Z 2023 *Chin. Phys. B* **32** 128501
[14] Leonard Jr. E, Beck M A, Nelson J, *et al*. 2019 *Phys. Rev. Appl.* **11** 014009
[15] Dalgaard M, Motzoi F, Sørensen J J and Sherson J 2020 *npj Quantum Inform.* **6** 6
[16] Jokar M R, Rines R and Chong F T 2021 *IEEE International Conference on Quantum Computing and Engineering (QCE)*, October 17–22, 2021, Broomfield, USA, pp. 402–412
[17] Jokar M R, Rines R and Chong F T 2022 *IEEE International Symposium on High-Performance Computer Architecture (HPCA)*, April 2–6, 2022, Seoul, Korea, pp. 400–414
[18] Wang Y F, Gao W P, Liu K, Ji B, Wang Z and Lin Z R 2023 *Phys. Rev. Appl.* **19** 044031
[19] Koch J, Yu T M, Gambetta J, Houck A A, Schuster D I, Majer J, Blais A, Devoret M H, Girvin S M and Schoelkopf R J 2007 *Phys. Rev. A* **76** 042319
[20] Barends R, Kelly J, Megrant A, *et al*. 2013 *Phys. Rev. Lett.* **111** 080502
[21] Geng X, He K, Liu J and Chen W 2023 *Front. Phys. Lausanne* **11** 1215468
[22] Yan F, Krantz P, Sung Y, Kjaergaard M, Campbell D L, Orlando T P, Gustavsson S and Oliver W D 2018 *Phys. Rev. Appl.* **10** 054062
[23] Rasmussen S E, Christensen K S, Pedersen S P, Kristensen L B, Bækkegaard T, Loft N J S and Zinner N T 2021 *PRX Quantum* **2** 040204
[24] Likharev K K 1986 *Dynamics of Josephson Junctions and Circuits* (London: CRC Press) p. 6
[25] He K, Dai G, Yu Q, He Y, Zhao C, Liu J and Chen W 2023 *Supercond. Sci. Technol.* **36** 045010
[26] Johansson J R, Nation P D and Nori F 2012 *Comput. Phys. Commun.* **183** 1760
[27] Johansson J R, Nation P D and Nori F 2013 *Comput. Phys. Commun.* **184** 1234
[28] Tibbetts K W M, Brif C, Grace M D, Donovan A, Hocker D L, Ho T, Wu R and Rabitz H 2012 *Phys. Rev. A* **86** 062309
[29] Nielsen M A and Chuang Isaac L 2010 *Quantum Computation and Quantum Information* (Cambridge: Cambridge University Press) p. 389
[30] Chuang I L and Nielsen M A 1997 *J. Mod. Optic.* **44** 2455
[31] Chow J M, Gambetta J M, Tornberg L, Koch J, Bishop L S, Houck A A, Johnson B R, Frunzio L, Girvin S M and Schoelkopf R J 2009 *Phys. Rev. Lett.* **102** 090502
[32] Nielsen M A 2002 *Phys. Lett. A* **303** 249
[33] Horodecki M, Horodecki P and Horodecki R 1999 *Phys. Rev. A* **60** 1888
[34] Barends R, Quintana C M, Petukhov A G, *et al*. 2019 *Phys. Rev. Lett.* **123** 210501